A Tough Silicon Nitride Ceramic with High Thermal Conductivity

You Zhou, Hideki Hyuga, Dai Kusano, Yu-ichi Yoshizawa, and Kiyoshi Hirao*

The world is shifting energy sources from fossil fuel to electric power in order to cope with the energy and environmental problems. Driven by the demand for efficient control and conversion of electric power, power electronic device technology is advancing toward higher voltage, larger current, greater power density, and smaller size, and this trend is poised to be accelerated with the replacement of Si by the wide-bandgap semiconductors (SiC and GaN) in the near future.[1,2] However, the high power will induce large thermal stresses in the devices, which pose great challenges for the assembly of the devices and the packaging materials, in particular the brittle ceramic substrates that provide functions of electrical insulation and heat dissipation. In many occasions, even the two high-grade ceramic substrate materials, AlN and Si_3N_4, become cracked due to low mechanical strength and fracture toughness (for AlN) or insufficient thermal conductivity (for Si_3N_4).[3,4] The reliability problem caused by the ceramic substrates has become a bottleneck hindering the advancement of power device technology. Search for new ceramic materials with better thermomechanical properties is an urgent issue. Here, we show a new Si_3N_4 ceramic that possesses a very high thermal conductivity (177 W m^{-1} K^{-1}) along with a high fracture toughness (11.2 MPa $m^{1/2}$) and a high fracture strength (460 MPa). We expect this Si_3N_4 will be used as the next-generation insulating substrate material for high-power electronic devices.

Silicon nitride mainly exists in two hexagonal polymorphs, namely α- and β-Si_3N_4, which are generally regarded as low- and high-temperature crystal forms, respectively.[5,6] As a highly covalent compound, Si_3N_4 transports heat primarily by phonons at room temperature and below. In 1995, Haggerty and Lightfoot predicted that the intrinsic thermal conductivity of Si_3N_4 might be 200 to 320 W m^{-1} K^{-1} at room temperature.[7] Later, Hirosaki et al. estimated that the intrinsic thermal conductivities of a β-Si_3N_4 crystal were 170 and 450 W m^{-1} K^{-1} along the *a*-axis and *c*-axis, respectively.[8] However, the thermal conductivity of Si_3N_4 ceramics is much lower than the intrinsic values. Si_3N_4 ceramics are polycrystalline materials consolidated by liquid-phase sintering. During sintering, Si_3N_4 raw powder, which is usually α phase, converts to the more stable β phase. In the microstructure of Si_3N_4 ceramics, grain boundary phases residing between β-Si_3N_4 grains and imperfections (impurity atoms, vacancies, dislocations, etc.), which exist in each β-Si_3N_4 grain, all act as factors that lower the thermal conductivity. Among them, as first reported by Kitayama et al., an oxygen impurity dissolved in the lattice of a β-Si_3N_4 grain, which creates phonon-scattering silicon vacancies, is regarded as the dominant extrinsic factor governing the thermal conductivity of Si_3N_4 ceramics.[9,10] Since the middle of 1990s, many research groups have engaged in preparing high-thermal-conductivity Si_3N_4 ceramics.[11] In those studies, the key approach for improving thermal conductivity was to remove lattice oxygen and enhance grain growth via the solution-reprecipitation mechanism by sintering high-purity Si_3N_4 powder at a high temperature for a long time. As a result, thermal conductivity could be improved, but the material developed a coarse microstructure that led to drastic decrease in mechanical strength. So far, the highest thermal conductivity (155 W m^{-1} K^{-1}) has been reported for a textured β-Si_3N_4 ceramic along the grain alignment direction, which was obtained by annealing at an extremely high temperature (2500 °C).[12] Nevertheless, such a high thermal conductivity has never been achieved in Si_3N_4 ceramics composed of randomly distributed grains.

For the Si_3N_4 starting powder, even the top high-purity commercial powder contains more than 1 wt% of oxygen that resides both on the surface and in the lattice, which imposes an upper limit on the attainable thermal conductivity of Si_3N_4 ceramics. In order to raise the upper limit to a higher level, a starting powder containing less oxygen should be used. Motivated by such an idea, we proposed a strategy for preparing high-thermal-conductivity Si_3N_4 via a route of sintering of reaction bonded silicon nitride (SRBSN), which is a well-known process of fabricating Si_3N_4 ceramics from Si starting powder instead of Si_3N_4 powder,[6,13] in consideration of the fact that Si powders that contain far fewer oxygen and metallic impurities than Si_3N_4 powders are commercially available because of the advancement of modern semiconductor industry. Our experimental results have verified the effectiveness of the SRBSN strategy, by which both higher thermal conductivity and higher strength were achieved, compared to the conventional sintering of silicon nitride powder (SSN) route.[14,15] We prepared a SRBSN material with a thermal conductivity of 133 W m^{-1} K^{-1}, however further improvement of thermal conductivity was difficult.[15] Although Hirao et al. predicted that Si_3N_4 ceramics free from lattice oxygen should have a thermal conductivity of at least 180 W m^{-1} K^{-1} using an extrapolation method,[16] it seemed too high to be experimentally realizable. Here, however, we show that a Si_3N_4 ceramic with a thermal conductivity as high as 177 W m^{-1} K^{-1} can be prepared by modifying the SRBSN process.

Dr. Y. Zhou, Dr. H. Hyuga, Dr. Y.-i. Yoshizawa, Dr. K. Hirao
National Institute of Advanced Industrial Science and Technology (AIST)
Nagoya 463-8560, Japan
E-mail: you.zhou@aist.go.jp
D. Kusano
Japan Fine Ceramics Co., Ltd
Sendai 981-3203, Japan

DOI: 10.1002/adma.201102462

As previously reported,[15] a high purity Si powder containing 0.28 wt% of oxygen with a mean particle size (d_{50}) of 8.5 μm was used as a starting material, and a mixture of Y_2O_3 (2 mol%) and MgO (5 mol%) was used as the sintering additive. The nitriding condition was modified by creating a more reducing atmosphere in the reaction zone and using a faster heating rate so as to obtain a higher β:α Si_3N_4 ratio, which we assumed might lead to higher thermal conductivity. The rationale of the assumption is that many studies since the 1970s have revealed that α-Si_3N_4 is able to accommodate various amounts of oxygen in its lattice,[17] but there was no report on the dissolution of oxygen in β-Si_3N_4 until the measurement reported by Kitayama et al. in 1999, which indicated that the oxygen dissolved in a β-Si_3N_4 crystal lattice is much less than the values reported for most α-Si_3N_4.[9] This suggests that a resultant β-Si_3N_4 crystal might accommodate less lattice oxygen than a resultant α-Si_3N_4 crystal when a reaction-bonded silicon nitride (RBSN) is prepared by nitridation of Si. If that is true, measures should be taken to enhance the formation of the β phase during nitridation so as to reduce the total lattice oxygen content, thereby improving the thermal conductivity of the prepared SRBSN material. Nevertheless, in the past researchers have always tried to promote the formation of α-Si_3N_4 in preparing a RBSN, based on the belief that the α-to-β phase transformation could enhance the anisotropic grain growth of β-Si_3N_4 grains during post-sintering,[6,13] thereby forming an interlocking microstructure composed of rod-like grains, which is crucial for attaining high fracture toughness.[18,19]

Full nitridation of a Si compact was achieved after heating to 1400 °C for 4 h under a nitrogen pressure of 0.1 MPa. The X-ray diffraction pattern of the nitrided compact (**Figure 1**a) showed that the main crystalline phase was β-Si_3N_4 and the minor crystalline phases were α-Si_3N_4 and $YSiO_2N$. Quantitative analysis revealed that the β:α ratio was 82.5:17.5. In contrast, the nitrided compact obtained under the nitriding conditions used in previous work had a β:α ratio of 59.8:40.2.[15] The higher β:α ratio of the RBSN could be attributed to the more reducing atmosphere in the reaction zone under this modified nitriding condition. A more reducing atmosphere led to a lower oxygen partial pressure, which could promote the formation of β-Si_3N_4 according to the thermodynamic analysis of Wild et al. on the nitridation reaction of Si.[20] Hereafter, these two kinds of nitrided compacts with high and low β:α ratios are referred to as high-β RBSN and low-β RBSN, respectively. As shown in Figure 1b, the microstructure of the high-β RBSN consisted of fine particles, among which the larger ones revealed elongated and faceted morphologies while the lengths were less than 2 μm. Compared to the low-β RBSN reported previously,[15] the microstructure of this high-β RBSN was slightly coarser and contained more elongated particles due to its higher β content. Lattice oxygen contents of the nitrided compacts were measured by the hot-gas extraction method according to the procedures described by Kitayama et al.[9] The lattice oxygen contents were 0.115 and 0.142 wt% for the high-β RBSN and low-β RBSN, respectively, which proved our assumption that lattice oxygen content of the resultant Si_3N_4 could be reduced by promoting the formation of the β phase during nitridation of Si.

Si_3N_4 ceramics were prepared by post-sintering the high-β RBSN compacts at 1900 °C under a nitrogen pressure of 1 MPa for various lengths of time. The materials sintered for 3, 6, 12, and 24 h were all fully densified and they had thermal conductivities of 109, 125, 146, and 154 W m^{-1} K^{-1}, respectively. In contrast, as previously reported, under the same post-sintering conditions the Si_3N_4 ceramics sintered from the low-β RBSN compacts for 3, 6, 12, and 24 h had thermal conductivities of 100, 105, 117, and 133 W m^{-1} K^{-1}, respectively.[15] The improvement in thermal conductivity of the Si_3N_4 sintered from the high-β RBSN over those sintered from the low-β RBSN was remarkable. Lattice oxygen measurements revealed that the Si_3N_4 sintered from the high-β RBSN for 3, 6, 12, and 24 h had lattice oxygen contents of 0.048, 0.041, 0.022, and 0.017 wt%, respectively. In contrast, the Si_3N_4 materials sintered from the low-β RBSN for 3, 6, 12, and 24 h in our previous study had lattice oxygen contents of 0.065, 0.057, 0.043, and 0.033 wt%, respectively. The decreasing lattice oxygen content with prolonged sintering time indicated that Si_3N_4 lattice was purified by the solution-reprecipitation mechanism, similar to the previous studies.[11] In addition, microstructural observations revealed that these two types of Si_3N_4 materials sintered for the same length of time had similar microstructures. Therefore, it is reasonable to attribute the higher thermal conductivities of the Si_3N_4 ceramics sintered from the high-β RBSN compared

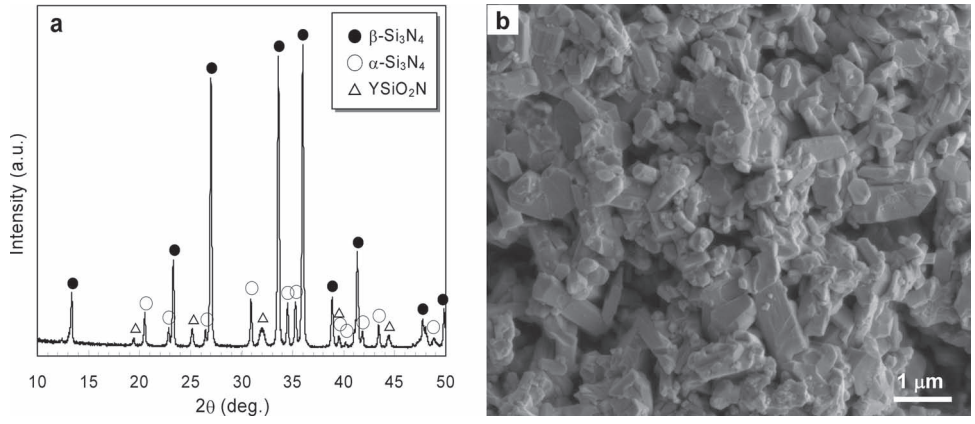

Figure 1. Characteristics of a high-β RBSN compact. a) X-ray diffraction pattern shows the crystalline phases in the nitrided compact. b) Scanning electron microscopy (SEM) image shows fine silicon nitride particles resulting from nitridation of a coarse Si powder.

to those sintered from the low-β RBSN to their lower lattice oxygen contents.

Encouraged by the advancement, we decided to post-sinter for longer times in order to see how high the thermal conductivity could become. Experimental results showed that when sintered at 1900 °C for 60 and 120 h, the Si_3N_4 ceramics attained thermal conductivities of 165 and 169 W m^{-1} K^{-1}, respectively, implying that it would be difficult to further improve the thermal conductivity to a higher level by solely prolonging sintering time. The lattice oxygen contents of the Si_3N_4 sintered for 60 and 120 h were 0.012 and 0.011 wt%, respectively. It seemed that the lattice oxygen content might have reached the lower limit that could be attained by long time sintering. Then, instead of prolonging sintering time we tried an annealing treatment, which was done by sintering a high-β RBSN at 1900 °C for 60 h followed by cooling at a very slow rate (0.2 °C min^{-1}), with the expectation that the annealing might help reduce structural imperfections in β-Si_3N_4 grains and enhance devitrification of amorphous grain boundary phases. It turned out that the Si_3N_4 prepared by this process attained a thermal conductivity of 177 W m^{-1} K^{-1}.

Figure 2 shows the microstructures of two representative Si_3N_4 ceramics prepared in this study: one was sintered for 3 h and the other was sintered for 60 h plus annealing. Sintering for 3 h resulted in a material with a bimodal microstructure, where a few large elongated grains dispersed in a matrix of fine grains (Figure 2a). Sintering for 60 h plus annealing led to a very coarse microstructure, where some large elongated grains had widths over 10 μm and lengths around 100 μm (Figure 2c). Higher magnification scanning electron microscopy (SEM) images revealed that the amount and the distribution state of the grain boundary phases in the microstructures of the two materials were different (Figure 2b,d). The material obtained by sintering for 60 h plus annealing contained fewer grain boundary phases than the material sintered for 3 h. Because a fraction of the liquid phase evaporated during sintering at 1900 °C and due to the longer sintering time, the more liquid phase was lost. The measured results showed that the weight loss values were 0.9 wt% and 3.8 wt% when sintering times were 3 and 60 h, respectively. Additionally, because the grain sizes of short-time-sintered material were smaller than those of the long-time-sintered material, the number of grain boundaries in a given volume for the former was larger than that for the latter. Furthermore, while in the short-time-sintered material most adjacent Si_3N_4 grains were separated by a thick film, in the long-time-sintered material only a few grain boundaries contained a thick film and most secondary phases resided at multigrain junctions. The decreased amount of grain boundary phases, decreased number of grain boundaries in concert with the increased Si_3N_4-Si_3N_4 contiguity in the long-time-sintered material should have contributed to the improvement in thermal conductivity. Nevertheless, it should be noted that the influences of such microstructural factors on thermal conductivity are secondary to the influence of lattice oxygen, as shown by previous studies.[11,21]

After achieving a thermal conductivity as high as 177 W m^{-1} K^{-1}, it became interesting and important to study the mechanical properties of the Si_3N_4 ceramic. As measured by the SEPB method, the Si_3N_4 showed a fracture toughness of 11.2 ± 0.4 MPa m$^{1/2}$. Although it is well known that Si_3N_4 is a champion ceramic material in terms of fracture toughness, a fracture toughness value as high as 11.2 MPa m$^{1/2}$ can seldom be found in the literature. Recently, Becher et al. reported similar high fracture toughness values for Si_3N_4 ceramics prepared by hot-pressing an α-Si_3N_4 powder doped with mixtures of RE_2O_3 (RE = La, Gd, and Lu) and MgO as sintering additives, but their thermal conductivity property was not mentioned.[22] The results of the present study reveal that starting with an α-Si_3N_4 powder is not an indispensable prerequisite for preparing tough β-Si_3N_4 ceramics, and high fracture toughness can be achieved by starting with a Si_3N_4 powder containing more than 80% β-phase if appropriate sintering additives and sintering conditions are chosen. Detailed studies will be needed to ascertain the reason behind the high fracture toughness of this material. However, preliminary microstructural analyses may provide clues to answer the question.

The SEM images shown in Figure 2 indicated that an interlocking microstructure composed of rod-like β-Si_3N_4 grains, which has been regarded as a necessity for attaining high fracture toughness, was formed even

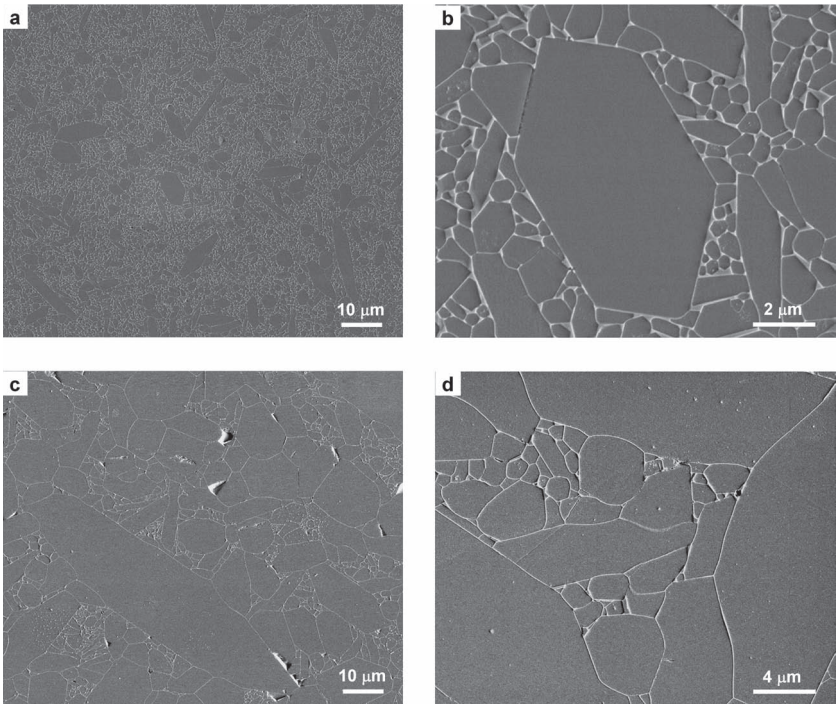

Figure 2. SEM images of the polished and plasma-etched surfaces of the Si_3N_4 ceramics obtained by post-sintering of a high-β RBSN compact at 1900 °C for various lengths of time. a,b) SEM images of a Si_3N_4 post-sintered for 3 h: a) low magnification image and b) high magnification image. c,d) SEM images of a Si_3N_4 post-sintered for 60 h plus annealing: c) low magnification image and d) high magnification image.

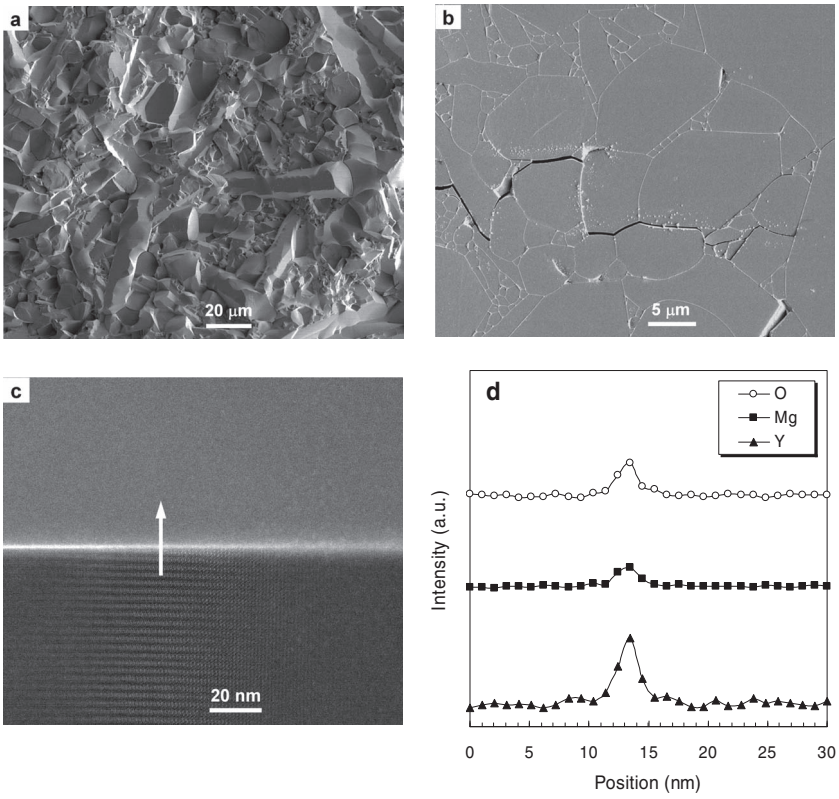

Figure 3. Microstructural features relating to the fracture behavior of a Si_3N_4 ceramic with a thermal conductivity of 177 W m^{-1} K^{-1} and a fracture toughness of 11.2 MPa $m^{1/2}$. a) SEM image of the fracture surface of the material. b) SEM view of a crack path (propagating from left to right) in the material. c) HAADF-STEM image showing a boundary between two adjacent Si_3N_4 grains. d) Compositional line profiles across the grain boundary shown in (c).

if 82.5% of the Si_3N_4 particles in the nitrided compact was β-phase. Observation of the fracture surface of the Si_3N_4 with a fracture toughness of 11.2 MPa $m^{1/2}$ revealed that the fracture mode was predominantly intergranular fracture (**Figure 3**a), indicating that the grain boundary strength was relatively weak. It is known that an appropriately weak grain boundary favors high fracture toughness because it can lead to interfacial debonding, which is necessary for facilitating the toughening effects such as crack bridging and crack deflection.[23–25] The SEM image of a crack path showed that the crack tortuously propagated in the material (Figure 3b), causing interfacial debonding and leading to crack deflection and crack bridging. The high angle annular dark-field scanning transmission electron microscopy (HAADF-STEM) image clearly showed that secondary phases containing elements other than Si and N resided at a boundary between two β-Si_3N_4 grains as a thin film (Figure 3c), and compositional line profiles probed by energy dispersive X-ray spectroscopy (EDX) across the boundary revealed that the grain boundary phases contained O, Mg, and Y elements, which were from the sintering additives (Figure 3d). It would be reasonable to assume that the existence of these grain boundary phases resulted in relative weak interfacial bonding between adjacent β-Si_3N_4 grains, which was important for achieving the high fracture toughness of the material. Furthermore, measured by a four-point bending test, the material showed a fracture strength of 460 ± 12 MPa. Considering the coarse microstructure of the material (as shown in Figure 2c), this strength was indeed rather high. The inevitable reduction in fracture strength caused by the existence of the large grains in the microstructure might have been alleviated by the improvement of fracture toughness.

The developed Si_3N_4 ceramic, which possesses a thermal conductivity of 177 W m^{-1} K^{-1}, bears comparison with AlN as a high-thermal-conductivity material. The three times higher fracture toughness and the higher fracture strength than AlN will make this Si_3N_4 a superior substrate material for future high-power electronic devices and other new applications. Moreover, the modified SRBSN method developed in this study has not only resulted in the achievement of the highest thermal conductivity but also suggests a possibility of bringing the thermal conductivity of Si_3N_4 to an even higher level.

Experimental Section

Materials Preparation: A high purity Si powder (Kojundo Chemical Laboratory) with a mean particle size (d_{50}) of 8.5 μm, a total metallic impurities content of less than 0.01 wt% and oxygen content of 0.28 wt% was used as the starting powder for the SRBSN process. High purity Y_2O_3 and MgO were used as sintering additives. The amount of sintering additives in the Si compact was determined so as to give the fully nitrided compact a nominal composition of Si_3N_4:Y_2O_3:MgO = 93:2:5 molar ratio. The Si and sintering additives were mixed in methanol using a planetary mill in a Si_3N_4 jar with Si_3N_4 balls. After vacuum drying and sieving, the mixed powder (about 18 g) was uniaxially pressed in a 45 mm × 45 mm stainless-steel die and then cold-isostatically pressed at a pressure of 300 MPa. The formed Si green compact with a dimension of around 41 mm × 41 mm × 7.2 mm and a relative density of about 61% was placed in a graphite resistance furnace and nitrided at 1400 °C for 4 h under a nitrogen pressure of 0.1 MPa. Post-sintering of the nitrided compact was done at 1900 °C under a nitrogen pressure of 1 MPa. Holding times at the sintering temperature ranged from 3 to 120 h. For the post-sintering, both heating rate and cooling rate were 10 °C min^{-1}, except in the case of annealing treatment when the cooling rate was 0.2 °C min^{-1}.

Characterization: The bulk density was measured using the Archimedes method. Phase identification for the nitrided and post-sintered materials was performed by X-ray diffraction analysis (XRD) (RINT2500, Rigaku). Quantitative analysis of α- and β-Si_3N_4 phases was carried out according to the method described by Pigeon and Varma.[26] Microstructures of fracture surfaces of the nitrided and post-sintered materials were observed using SEM (JSM-6340F, JEOL). Microstructures were also observed by SEM on the polished and plasma etched (by a CF_4 gas) surfaces so as to reveal the morphologies and distribution states of the β-Si_3N_4 grains and grain boundary phases. Indentations were placed on the polished surfaces by a Vickers indenter to introduce cracks, and then the indented surfaces were plasma etched and observed by SEM to examine the crack/microstructure interactions. HAADF-STEM images were acquired using a FEI Titan80-300 operating at 300 kV, and compositional line profiles were probed by EDX.

Lattice Oxygen Analysis: Lattice oxygen content was determined according to the method reported by Kitayama et al.[9,10] Approximately 1 g of sample was cut from a nitrided or post-sintered compact, followed by pulverizing with a tungsten carbide vibration mill. The milled powder was treated first with 50% HF at 60 °C for 3 h and then with 50% H_2SO_4 at 120 °C for 2 h to remove the secondary phases and the oxidized surface layers on the milled particles. After washing with distilled water, each powder was dried at 110 °C for 12 h and passed through a 100 mesh sieve. A powder sample (about 20 mg) was loaded into a graphite crucible, which was then set in a hot-gas extraction analyzer (Model TC-436, LECO) and heated to 2500 °C in 5 min. The release of oxygen and nitrogen as a function of temperature was recorded. Gaussian peak separation was performed so as to separate the oxygen counts released from the Si_3N_4 lattice and those from the surface of Si_3N_4 particles, thereby determining the oxygen content within the Si_3N_4 lattice.

Properties Measurement: Test beams with dimensions of 4 mm × 3 mm × 36 mm were sectioned and ground with a 400-grit diamond grinding wheel. Fracture strength was determined on the beams tested in a four-point bending jig with an outer span of 30 mm and an inner span of 10 mm. Fracture toughness was determined by the single-edge-precracked-beam method (SEPB) method.[27] Thermal diffusivity and specific heat were measured using the laser flash method (Model TC-7000, ULVAC) and thermal conductivity was calculated using the measured values of thermal diffusivity, specific heat, and bulk density.

Acknowledgements

The authors thank A. Tsuge of AIST for help in measuring oxygen content.

Received: June 28, 2011
Revised: July 29, 2011
Published online: September 8, 2011

[1] H. Okumura, *Jpn. J. Appl. Phys.* **2006**, *45*, 7565.
[2] C. R. Eddy Jr., D. K. Gaskill, *Science* **2009**, *324*, 1398.
[3] H. Lu, C. Bailey, C. Y. Yin, *Microelectron. Reliab.* **2009**, *49*, 1250.
[4] C. Buttay, D. Planson, B. Allard, D. Bergogne, P. Bevilacqua, C. Joubert, M. Lazar, C. Martin, H. Morel, D. Tournier, C. Raynaud, *Mater. Sci. Eng. B* **2011**, *176*, 283.
[5] S. Hampshire, H. K. Park, D. P. Thompson, K. H. Jack, *Nature* **1978**, *274*, 880.
[6] F. L. Riley, *J. Am. Ceram. Soc.* **2000**, *83*, 245.
[7] J. S. Haggerty, A. Lightfoot, *Ceram. Eng. Sci. Proc.* **1995**, *16*, 475.
[8] N. Hirosaki, S. Ogata, C. Kocer, H. Kitagawa, Y. Nakamura, *Phys. Rev. B* **2002**, *65*, 134110.
[9] M. Kitayama, K. Hirao, A. Tsuge, M. Toriyama, S. Kanzaki, *J. Am. Ceram. Soc.* **1999**, *82*, 3263.
[10] M. Kitayama, K. Hirao, A. Tsuge, K. Watari, M. Toriyama, S. Kanzaki, *J. Am. Ceram. Soc.* **2000**, *83*, 1985.
[11] K. Hirao, Y. Zhou, in *Ceramics Science and Technology*, (Eds: R. Riedel, I.-W. Chen), Wiley-VCH, Weinheim, Germany **2010**, Vol. *2*, pp. 667–696.
[12] K. Watari, K. Hirao, M. E. Brito, M. Toriyama, S. Kanzaki, *J. Mater. Res.* **1999**, *14*, 1538.
[13] G. Ziegler, J. Heinrich, G. Wotting, *J. Mater. Sci.* **1987**, *22*, 3041.
[14] X. W. Zhu, Y. Zhou, K. Hirao, Z. Lences, *J. Am. Ceram. Soc.* **2006**, *89*, 3331.
[15] Y. Zhou, X. W. Zhu, K. Hirao, Z. Lences, *Int. J. Appl. Ceram. Technol.* **2008**, *5*, 119.
[16] K. Hirao, K. Watari, H. Hayashi, M. Kitayama, *MRS Bull.* **2001**, *26*, 451.
[17] C. M. Wang, X. Q. Pan, M. Ruhle, F. L. Riley, M. Mitomo, *J. Mater. Sci.* **1996**, *31*, 5281.
[18] I.-W Chen, A. Rosenflanz, *Nature* **1997**, *389*, 701.
[19] Z. J. Shen, Z. Zhao, H. Peng, M. Nygren, *Nature* **2002**, *417*, 266.
[20] S. Wild, P. Grieveson, K. H. Jack, in *Special Ceramics*, (Ed: P. Popper), British Ceramic Research Association, Stoke-on-Trent, UK **1972**, Vol. *5*, pp. 271–284.
[21] M. Kitayama, K. Hirao, K. Watari, M. Toriyama, S. Kanzaki, *J. Am. Ceram. Soc.* **1999**, *82*, 3105.
[22] P. F. Becher, G. S. Painter, N. Shibata, S. B. Waters, H.-T. Lin, *J. Am. Ceram. Soc.* **2008**, *91*, 2328.
[23] P. F. Becher, *J. Am. Ceram. Soc.* **1991**, *74*, 255.
[24] H.-J. Kleebe, G. Pezzotti, G. Ziegler, *J. Am. Ceram. Soc.* **1999**, *82*, 1857.
[25] R. L. Satet, M. J. Hoffmann, *J. Am. Ceram. Soc.* **2005**, *88*, 2485.
[26] R. G. Pigeon, A. Varma, *J. Mater. Sci. Lett.* **1992**, *11*, 1370.
[27] T. Nose, T. Fujii, *J. Am. Ceram. Soc.* **1988**, *71*, 328.